ACS OMEGA

Open Access

http://pubs.acs.org/journal/acsodf

Article

Ultrasound-Targeted Microbubble Destruction Enhances the Inhibitory Effect of Sonodynamic Therapy against Hepatocellular Carcinoma

Huajing Yang, Yunfeng Qu, Yuhang Tian, Chunyue Wang, Yucao Sun, Zhifei Dai,* Xiuli Yue,* and Wen Cheng*

Cite This: *ACS Omega* 2024, 9, 51253−51263

Read Online

ACCESS | Metrics & More | Article Recommendations | Supporting Information

ABSTRACT: *Purpose*: To assess the anticancer effect of microbubbles (MBs) in combination with sinoporphyrin sodium (DVDMS)-mediated sonodynamic therapy (SDT) for the in vitro and in vivo treatment of hepatocellular carcinoma (HCC). *Methods*: HepG2 cells were used for in vitro experiments. Reactive oxygen species (ROS) production was detected using 2′,7′-dichlorodihydrofluorescein diacetate and singlet oxygen sensor green in vitro and in solution, respectively. Cytotoxicity was evaluated using a Cell Counting Kit 8 assay and the calcein AM/PI double-staining method. Annexin V-FITC/PI staining was employed to analyze the rate of cell apoptosis. Cell surface calreticulin exposure, high mobility group box 1 release, and adenosine triphosphate secretion were measured to detect immunogenic cell death (ICD). The anticancer effect of the combination therapy was further assessed in Hepa1−6 tumor-bearing mice. *Results*: Compared with SDT alone, ROS production in the MBs + SDT group was enhanced 1.2-fold ($p < 0.0001$). The cytotoxic effect of DVDMS-mediated SDT on HepG2 cells was concentration-dependent, and the additional application of MBs increased cytotoxicity. Additionally, MBs augmented the SDT-induced apoptosis rate from 33.26 ± 13.48 to 72.95 ± 7.95% ($p < 0.01$). Notably, our results demonstrated that MBs can enhance SDT-induced ICD. In in vivo experiments, SDT combined with MBs significantly reduced tumor volume, with negligible differences in mouse body weight. Furthermore, MBs effectively enhanced SDT-induced tumor tissue destruction. *Conclusion*: The present study indicates that MBs can markedly improve the anticancer effects of SDT in HCC.

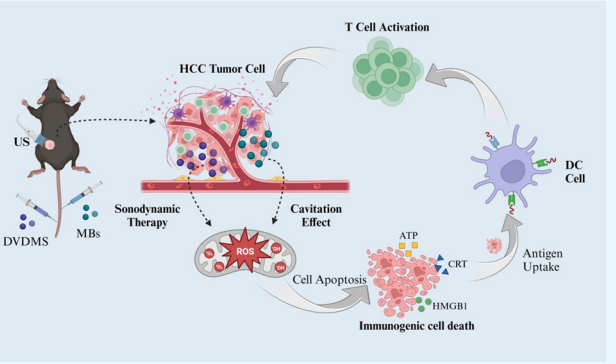

INTRODUCTION

Hepatocellular carcinoma (HCC) is the most common malignant tumor in the liver, the fourth most common cause of cancer-related death, and the sixth most common cancer globally.[1,2] Surgical resection, liver transplantation, and radiofrequency ablation are major treatment options for HCC.[3,4] However, patients with HCC are often in the advanced stage of the disease when they are diagnosed, rendering locoregional therapy ineffective; accordingly, patients with HCC typically have poor prognosis.[5,6] Therefore, it is of great clinical importance to identify other effective strategies for the treatment of HCC, overcoming the limitations of existing treatments.

Sonodynamic therapy (SDT) is a representative and promising noninvasive modality for tumor therapy.[7,8] Since ultrasound (US) can penetrate deep tissues and target regions of tumor growth, SDT addresses the drawback of photodynamic therapy (PDT), where the therapeutic effect is limited by insufficient light penetration depth.[9−11] Boron neutron capture therapy (BNCT) is a cell-selective radiotherapy that effectively treats tumors by inducing DNA breaks.[12,13] According to Hosmane's book, BNCT and gadolinium neutron capture therapy (GdNCT) have substantial clinical application potential in treating malignant tumors.[14] Compared to BNCT, SDT has no radiotoxicity and is applicable to various tumor treatments. The most accepted therapeutic mechanisms of SDT are acoustic cavitation, sonoluminescence, and pyrolysis.[15,16] When US-activated sonosensitizers return to their ground state, large amounts of energy are released and transferred into the surrounding oxygen, producing high levels of reactive oxygen species (ROS), including singlet oxygen ($^1O_2$).[16] Excessive ROS was reported to kill tumor cells by

Received: August 22, 2024
Revised: November 16, 2024
Accepted: November 28, 2024
Published: December 18, 2024

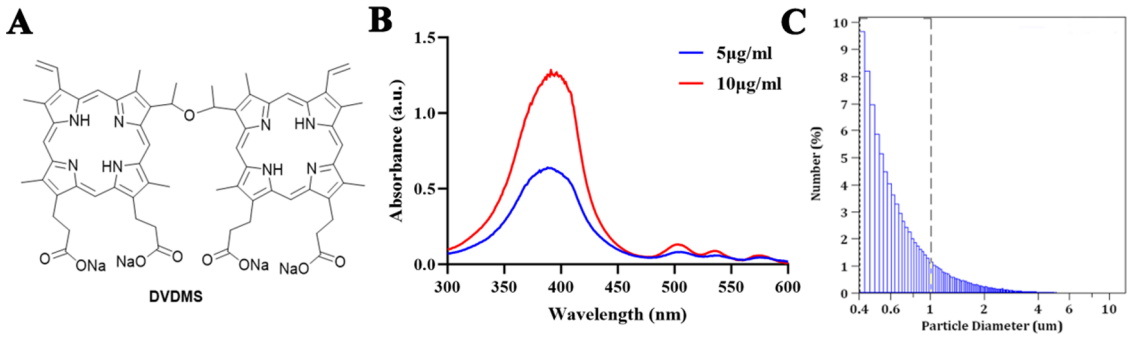

Figure 1. (A) Chemical structure of DVDMS. (B) Absorption spectrum of DVDMS. (C) Particle size of Feriview microbubbles.

affecting cell signaling, triggering mitochondrial apoptosis, and inducing damage to DNA.[17,18] Many sonosensitizers, such as hematoporphyrin monomethyl ether and chlorin-e6, are used in SDT.[19,20] Sinoporphyrin sodium (DVDMS) is a novel photo and sonosensitizer that was first isolated from Photofrin II by Fang et al.[21] of the Chinese Academy of Medical Sciences.[22] It possesses good chemical purity and water solubility with minimal dark toxicity and, therefore, has relatively short-term skin sensitivity and a high singlet oxygen-producing potential.[23,24] Previous studies using the High-Performance Liquid Chromatography method have demonstrated that DVDMS exhibits good stability in solution.[25] ROS-mediated SDT exerts cytotoxic effects by directly eliminating cancer cells and inducing immunogenic cell death (ICD).[26−28] It was reported that ICD leads to the release of tumor-associated antigens and substantial damage-associated molecular patterns from apoptotic or necrotic tumor cells and then promotes the recruitment and activation of antigen-presenting cell populations.[29,30] However, due to the hypoxia and immunosuppressive tumor microenvironment of HCC, SDT alone may not be sufficient to eradicate the tumor and may need to be supplemented by other therapies to enhance the cytotoxicity and tumor inhibition effect.[31]

Ultrasound-targeted microbubble destruction (UTMD) utilizes established short-pulse acoustic wave destruction of abnormal tumor vessels, enhances drug accumulation and intracellular uptake, and significantly improves therapeutic efficacy.[32,33] Gas-filled microbubbles (MBs), which are widely used in medical diagnosis as contrast agents for assessing blood perfusion in tumors, also play an important role in UTMD.[34,35] The shells of MBs are usually composed of polymers and lipids, and their nuclei are filled with inert polymolecular gases. Thus, MBs can act as ultrasonic response cavity nuclei in SDT to facilitate cavitation.[36] Since SDT is mediated by the combination of sonosensitizers with US-induced cavitation, MBs combined with sonosensitizers have been reported to effectively augment the antitumor effect and inhibit cancer progression compared to sonosensitizers alone.[37,38] Under sono-irradiation, MBs are forced to expand and contract, and the shock waves generated in this process enhance the permeability of the plasma membrane by inducing temporary pores in the cell membrane, thereby promoting cellular uptake of therapeutic agents, including sonosensitizers, in a process termed the sonoporation effect.[39,40] Oxidative stress that occurs during this process produces free radicals and intracellular ROS, inducing cell necrosis and apoptosis.[41,42] Furthermore, as MBs are suitable for contrast-enhanced US imaging of liver disease, their combination with SDT facilitates an integrated diagnosis and treatment.

In the present study, we focused on the combined effects of DVDMS-mediated SDT and UTMD on HCC treatment in vitro and in vivo. Our results revealed that MBs increased ROS production during SDT, leading to decreased HepG2 cell activity and increased apoptosis. The safety and effectiveness of the combination therapy were validated using a xenograft model.

MATERIALS AND METHODS

Reagents. Sinoporphyrin sodium (DVDMS, molecular formula: $C_{68}H_{66}N_8O_9Na_4$, molecular weight: 1231.28; purity: 99.3%) was provided by Shanghai Guangsheng Biopharmaceutical Co., Ltd. The chemical structure and absorption spectrum of DVDMS are shown in Figure 1A,B. After dissolving the DVDMS at a concentration of 10 mg/mL in DMSO, it was stored in the dark at 4 °C. Feriview microbubbles with lipid shells and C_3F_8 as the core gas were provided by Beijing Feirida Medical Technology Co. Ltd. This product is in the premarketing phase and is currently undergoing phase 3 clinical trials. This is the first study to use Feriview microbubbles to enhance the therapeutic effects of SDT. The particle size of the Feriview microbubbles is shown in Figure 1C, and most microbubbles have a particle size of less than 1 μm. A microbubble suspension was prepared using 1 mL of sterile 0.9% NaCl solution and mechanically vibrated for 45 s (approximately 7×10^9 microbubbles/mL). An ultrasound therapy instrument, Sonic-Stimu Pro UT1041, was purchased from Nu-tek Medical Company (Shenzhen, China). Cell Counting Kit-8 (CCK-8) and 2′,7′-dichlorodihydrofluorescein diacetate (DCFH-DA) assay kits were purchased from MedChemExpress (Shanghai, China). The singlet oxygen sensor green (SOSG) assay kit was supplied by Meilunbio (Beijing, China). The Calcein AM/propidium iodide (PI) Cell Viability/Cytotoxicity Assay Kit and enhanced adenosine triphosphate (ATP) assay kit were obtained from Beyotime Biotechnology (Jiangsu, China). The Annexin V-FITC Apoptosis Detection Kit was purchased from BD Biosciences (Franklin Lakes, NJ, US). Calreticulin (CRT) and high mobility group box 1 (HMGB1) antibodies were purchased from Abcam (Shanghai, China).

Cell Culture and Animal Model. Human and mouse HCC cell lines HepG2(Cat No.: CL-0103) and Hepa1−6 (Cat No.: CL-0105) were purchased from Procell Life Science &Technology Co., Ltd. (Wuhan, China) and cultured in Dulbecco's modified Eagle's medium (Gibco, Carlsbad, USA) supplemented with 10% fetal bovine serum (Vivacell Biosciences, Shanghai, China) and 1% penicillin/streptomycin (Gibco, Carlsbad, USA). Cells were cultured at 37 °C in humidified air containing 5% CO_2.

https://doi.org/10.1021/acsomega.4c07746
ACS Omega 2024, 9, 51253−51263

Thirty female C57BL/6 mice, aged 6−8 weeks and weighing 16−20 g, were selected for this experiment. The mice were purchased from Vital River Laboratory Animal Technology Co., Ltd. (Beijing, China) and kept in a specified pathogen-free environment. The subcutaneous tumor model of HCC was established according to published literature.[43] Hepa1−6 cells were digested, washed once using phosphate-buffered saline (PBS) buffer, resuspended in PBS with the cell density adjusted to 1×10^7 cells/mL, and placed on ice. After anesthesia of the C57BL/6 mice, the depilated skin was slightly clamped up using tweezers, and the cell suspension was aspirated using a 1 mL syringe, which was slowly inserted into the subcutaneous space and pulled out slowly after a 100 μL injection to prevent leakage of fluid. When the tumor volume increased to approximately 100 mm^3, the mice were ready for treatment experiments. All animal experiments complied with the ARRIVE guidelines and were carried out in accordance with The Animals (Scientific Procedures) Act 1986. All animal experiments were conducted according to the protocol approved by the Institutional Animal Care and Use Committee of Peking University (approval number: FT-DaiZF-4).

Reactive Oxygen Species Detection in Solution and In Vitro. After the HepG2 cells were trypsinized, they were placed into 6-well plates at a density of 3×10^5 cells/well and placed in an incubator overnight, and then divided into four groups: (a) NC (untreated control), (b) DVDMS, (c) SDT, and (d) MBs + SDT. The concentrations of DVDMS and MBs used for cell experiments were 5 μM and 3.5×10^7 microbubbles/mL, respectively, except for special markings. According to published literature, HepG2 cells were incubated with DVDMS for 5 h.[44] The DCFH-DA dilution was configured using serum-free medium to achieve a final concentration of 5 mM, 1 mL of configured dilutions of DCFH-DA was added to each well, and the wells were incubated in the dark for 30 min at 37 °C before ultrasound sonication. To prevent adherent cells from falling off the plate due to excessive ultrasonic oscillations, the ultrasound treatment for cell experiments was set at an acoustic intensity of 0.5 W/cm^2, a frequency of 1 MHz, and a duty cycle of 10% for 2 min. After different treatments, cells were washed with serum-free medium three times and observed by fluorescent microscopy (Nikon, Tokyo, Japan).

Singlet oxygen detection in solution was performed using SOSG. SOSG was dissolved to a concentration of 5 mM using methanol. The respective drugs in the different treatment groups were diluted to the above concentrations with PBS, and SOSG solutions of 5 μM concentration were added. After ultrasound irradiation (0.5 W/cm^2, 1 MHz, 10% duty cycle, 2 min), the fluorescence intensity of SOSG was analyzed using a fluorescence spectrophotometer (HITACHI, Tokyo, Japan).

In Vitro Cellular Uptake of DVDMS Assay. After the HepG2 cells were trypsinized, they were seeded into 6-well plates at a density of 3×10^5 cells/well and incubated overnight. After applying different treatments, the cells were harvested and washed three times with PBS, and cellular uptake of DVDMS was determined using flow cytometry (Becton, Dickinson and Company, New Jersey, USA).

Cytotoxicity Analysis. After the HepG2 cells were trypsinized, they were placed in 96-well plates at a density of 5×10^3 cells/well, and cytotoxicity was assessed using the CCK-8 method.[45] After different treatments for 24 h, 10 μL of the CCK-8 reagent was added to each well and incubated in the dark for 60 min. Subsequently, the optical density was measured using a microplate reader at 450 nm wavelength. Cell viability was evaluated using a Calcein AM/PI Cell Viability/Cytotoxicity Assay Kit. HepG2 cells precultured in six-well plates were treated and incubated for another 24 h. Fresh medium containing Calcein AM (5 μM) and PI (5 μM) was used to replace the original culture medium in each group. After three washes with serum-free medium, a fluorescence microscope was then used to observe the stained cells.

Cell Apoptosis Analysis. After the HepG2 cells were trypsinized, they were placed into 6-well plates at a density of 4×10^5 cells/well, and cell apoptosis was assessed using the Annexin V-FITC Apoptosis Detection Kit 24 h after different treatments.[46] The digested cells were suspended in 100 μL of 1× binding buffer; 5 μL of Annexin V-FITC and 5 μL of PI were then added and coincubated for 15 min in the dark at 25 °C. After staining, 400 μL of 1× binding buffer was added before flow cytometry. The data were analyzed using FlowJo_V10 software.

Detection of ICD Molecules. HepG2 cells were placed in confocal dishes at a density of 3×10^5 cells/dish followed by treatment, as mentioned above. After 24 h of incubation, the cells were stained with anti-CRT/HMGB1 antibody.[47] Nuclear staining was performed using 4′,6-diamidino-2-phenylindole (DAPI), and images were captured with confocal laser scanning microscopy following three washes with PBS. Additionally, the cells were digested for flow cytometric analysis.

For the ATP secretion assay, HepG2 cells were plated in 96-well plates at a concentration of 5×10^3 cells/well and incubated overnight. Subsequently, the cells were treated as described above. Once the supernatant was collected, dead cells were eliminated by centrifugation (1000 rpm, 4 min, 25 °C). An enhanced ATP assay kit was used to detect ATP secretion using a luminometer.

In Vivo Antitumor Effect Evaluation. For antitumor treatment analysis, Hepa1−6 tumor-bearing mice were divided into six groups (n = 5 per group): (a) NC, (b) US, (c) DVDMS, (d) MBs + US, (e) SDT, and (f) MBs + SDT. Treatment protocols were partly based on published articles.[48] DVDMS was administered at a dose of 2.5 mg/kg through caudal vein injection 12 h before ultrasound sonication, and 50 μL of MBs was intravenously injected immediately before ultrasound sonication. The mice were treated with ultrasound on days 1, 3, and 5. According to existing literature, the ultrasound parameters were set at an acoustic intensity of 3 W/cm^2, a frequency of 1 MHz, and a duty cycle of 50% for 5 min. Tumor development and mice weights were observed and recorded every other day until day 14. The formula for tumor volume calculation was as follows: volume = (Length × $Width^2$)/2 mm^3. On the 15th day after therapy, mice were euthanized, and tumors were collected and placed in 4% paraformaldehyde for 24 h. Hematoxylin and eosin (H&E) staining, Ki67 staining, and transferase dUTP nick end labeling (TUNEL) staining were performed to test for therapeutic efficacy. Quantitative analysis of Ki67 and TUNEL staining images was performed using ImageJ software.

Statistical Analysis. To ensure accuracy, each experiment was repeated under the same conditions at least three times. Statistical analysis of the experimental data was performed using the GraphPad Prism 10 software. All data are presented as mean ± SD, and $p < 0.05$ was considered statistically significant. t tests were used to compare data between two groups, and one-way analysis of variance (one-way ANOVA)

https://doi.org/10.1021/acsomega.4c07746
ACS Omega 2024, 9, 51253−51263

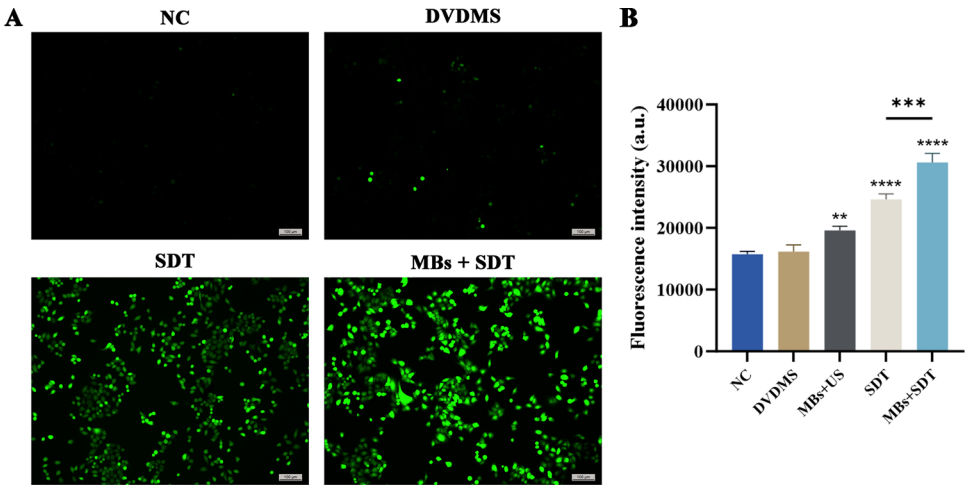

Figure 2. Detection of ROS production. (A) Fluorescence images of ROS generation in HepG2 cells indicated by a DCFH-DA probe. Scale bar: 100 μm. (B) Quantitative analysis of fluorescence intensity for singlet oxygen production in solution using SOSG. ** $p < 0.01$, *** $p < 0.001$, and **** $p < 0.0001$ compared to NC group.

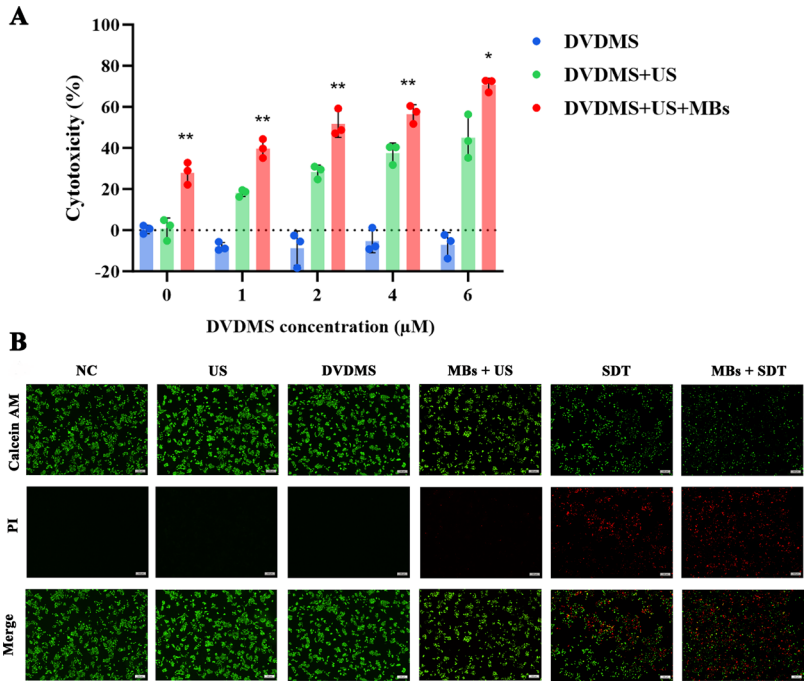

Figure 3. Microbubbles enhanced SDT-associated cytotoxicity. (A) Cytotoxicity of different treatments on HepG2 cells detected by a CCK-8 assay. *$p < 0.05$, **$p < 0.01$, compared to the SDT group. (B) Fluorescence images of HepG2 cells stained with Calcein AM (green fluorescence, representing living cells) and PI (red fluorescence, representing dead cells) after different treatments. Scale bar: 100 μm.

was used to compare data between multiple experimental groups.

RESULTS

Detection of ROS Production. Since intracellular ROS production is the most important mechanism for SDT, we investigated whether MBs could enhance the DVDMS-mediated SDT effect by detecting intracellular ROS generation in HepG2 cells using the cell-permeable fluorescent probe DCFH-DA. As shown in Figure 2A, minimal fluorescent signals were observed in the untreated control and DVDMS groups, whereas the ROS fluorescence of SDT-treated cells was much stronger. Moreover, the MBs + SDT group exhibited the highest ROS production, which was significantly higher than that observed with SDT alone.

To explore the mechanisms underlying increased ROS generation after MBs + SDT treatment, cellular uptake of UTMD-facilitated DVDMS was detected using flow cytometry. As shown in Figure S1, MBs effectively promoted DVDMS uptake by HepG2 cells under ultrasonic irradiation ($p < 0.0001$). Subsequently, we used the fluorescent probe SOSG to investigate whether the presence of MBs enhanced the production of singlet oxygen during SDT in a cell-free system. As shown in Figure 2B, the combination of MBs and US promoted intracellular ROS production ($p < 0.01$). Compared to the groups without ultrasound sonication, the SDT group demonstrated a 56.38 ± 8.21 and 52.79 ± 10.22% increase in

https://doi.org/10.1021/acsomega.4c07746
ACS Omega 2024, 9, 51253−51263

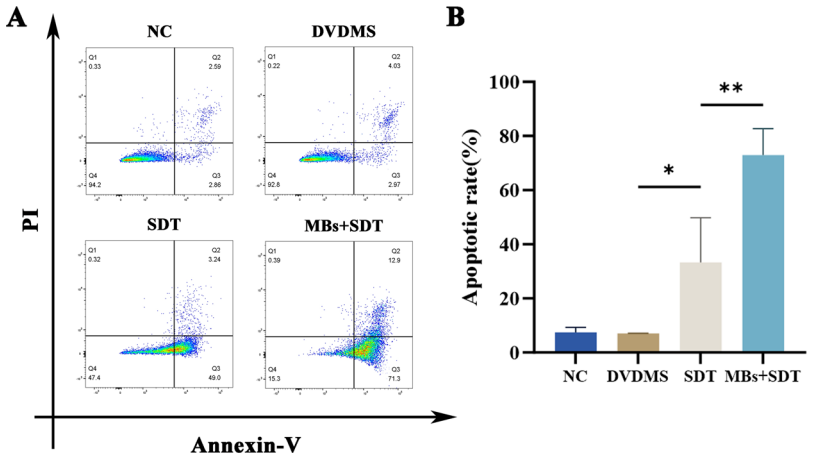

Figure 4. A combination of MBs and SDT induced HepG2 cell apoptosis. (A) Dot plots of HepG2 cell apoptosis using Annexin V-FITC and PI staining by flow cytometry. (B) MBs increased SDT-induced HepG2 cell apoptosis rate. *p < 0.05, **p < 0.01.

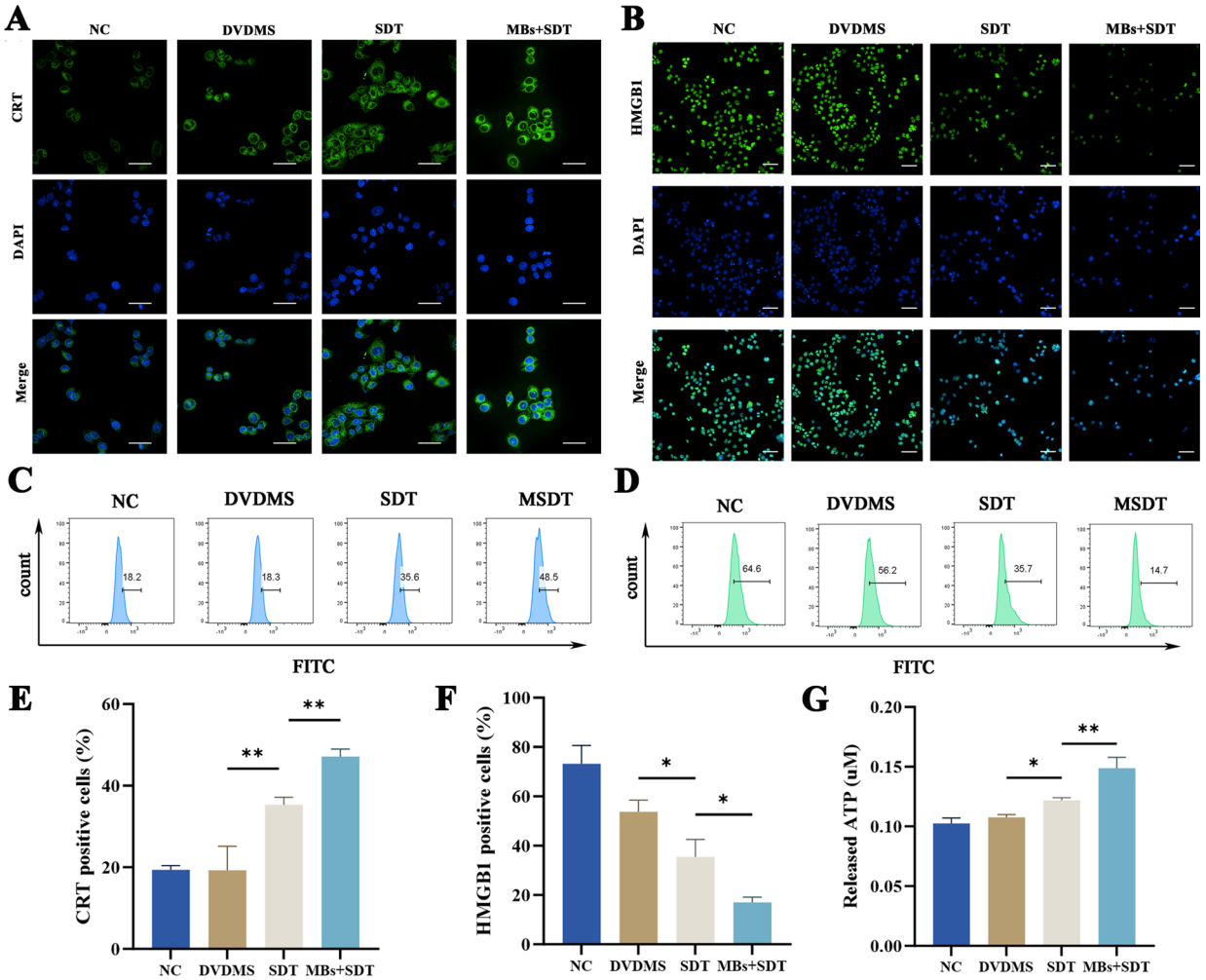

Figure 5. Evaluation of ICD in vitro. (A) Images of CRT exposure on the cell surface captured using confocal laser scanning microscopy. Scale bar: 50 μm. (B) Confocal laser scanning microscopy images of HMGB1 release in HepG2 cells. Scale bar: 100 μm. (C) Flow cytometry analysis of cell surface CRT exposure. (D) Flow cytometry analysis of intracellular HMGB1 expression. (E) Quantification analysis of CRT-positive cells (n = 3). **p < 0.01. (F) Quantification analysis of HMGB1 positive cells (n = 3). *p < 0.05. (G) The release of ATP in the cell culture medium from HepG2 cells (n = 3). *p < 0.05, **p < 0.01.

average fluorescence intensity, respectively. In addition, compared with SDT alone, the fluorescence intensity of MBs + SDT was enhanced 1.2-fold (p < 0.0001). These data demonstrate that adding MBs during SDT results in significantly higher ROS levels through UTMD.

https://doi.org/10.1021/acsomega.4c07746
ACS Omega 2024, 9, 51253−51263

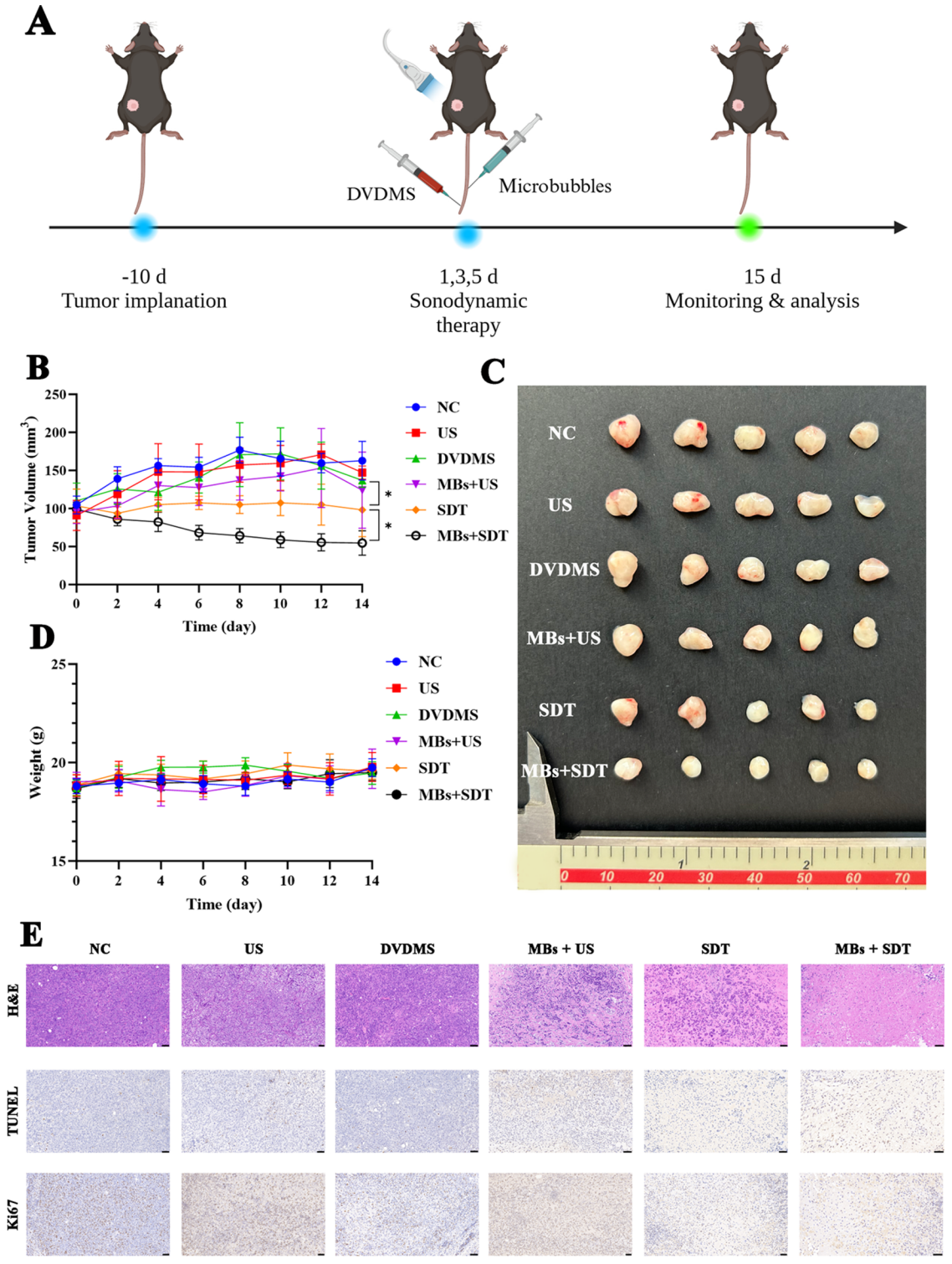

Figure 6. Evaluation of antitumor effect in vivo. (A) Schematic of antitumor study on hepa1−6 tumor mice. Created in BioRender. Zhao, C. (2023) BioRender.com/l66h355. (B) Tumor growth curves in the different groups (n = 5). (C) Images of corresponding tumors at the end of treatment. (D) Body weight curve of Hepa1−6 tumor-bearing mice (n = 5). (E) Histological images of H&E, TUNEL, and Ki67 staining revealed tissue damage, apoptosis, and cell proliferation, respectively. Scale bar: 50 μm.

Microbubbles Enhanced SDT-Associated Cytotoxicity. It has been reported that the production of intracellular ROS may be closely related to the cytotoxic effect induced by the sonosensitizer in the acoustic field. Therefore, the cytotoxicity of combined MBs and DVDMS under US irradiation was subsequently evaluated using the CCK-8 assay. As shown in Figure 3A, DVDMS or ultrasound alone did not demonstrate a marked effect on cytotoxicity, whereas their combination inhibited HepG2 cell proliferation in a dose-dependent manner. Notably, MBs under ultrasonication also inhibited HepG2 cell proliferation owing to UTMD, resulting in cytotoxicity of 27.97 ± 4.45%. Moreover, cytotoxicity was

https://doi.org/10.1021/acsomega.4c07746
ACS Omega 2024, 9, 51253−51263

significantly higher in the combination of MBs plus SDT group than in the single SDT group, with the IC_{50} value of DVDMS decreasing from 8.004 to 1.943 μM.

Furthermore, costaining with Calcein AM (green fluorescence, Ex/Em = 494/517 nm, representing living cells) and PI (red fluorescence, Ex/Em = 535/617 nm, representing dead cells) was also evaluated by fluorescence microscopy to reveal the antitumor effects of different treatments. The cells irradiated with or without US exhibited strong green fluorescence (Figure 3B). A similar phenomenon was observed in cells incubated with DVDMS in the absence of ultrasonication. However, the SDT and MBs + SDT groups demonstrated stronger red fluorescence and significant cytotoxicity, whereas the MBs + US group only demonstrated spotted red fluorescence.

Combination of MBs and SDT-Induced HepG2 Cell Apoptosis. According to published literature, when the cytotoxic ROS produced by SDT destabilizes the mitochondrial membrane, the released cytochrome C binds to an apoptosis protein activator in the cytoplasm, resulting in apoptosis.[49] Additionally, the sonotoxicity of UTMD has also been reported to induce cell apoptosis.[50] To explore the therapeutic mechanism of SDT in combination with MBs, Annexin V-FITC and PI staining were used to analyze HepG2 cell apoptosis (Figure 4). Compared with the control group or DVDMS alone, SDT treatment led to significant cellular apoptosis, predominantly early apoptosis. Furthermore, MBs enhanced cell apoptosis induced by the SDT process, as the apoptotic rate increased from 33.26 ± 13.48 to 72.95 ± 7.95% ($p < 0.01$). These results indicated that MBs increased SDT-induced HepG2 cell apoptosis.

Evaluation of ICD In Vitro. In addition to inducing cell necrosis and apoptosis, intracellular ROS can significantly trigger ICD, thereby initiating antitumor immune responses. Moreover, the ICD process could be characterized by the upregulated expression of CRT on the cell surface, increased extracellular HMGB1 release, and secretion of ATP. ICD-associated biomarkers were evaluated to investigate the role of ICD in combination with SDT and MBs. As indicated in the confocal laser scanning microscopy images in Figure 5A, HepG2 cells treated with DVDMS demonstrated slightly increased CRT exposure, whereas HepG2 cells treated with SDT with or without MBs demonstrated higher green fluorescence intensity. Flow cytometry analysis confirmed that CRT exposure was most pronounced in HepG2 cells after SDT and MBs + SDT treatments (Figure 5C,E).

The confocal laser scanning microscopy image in Figure 5B shows that intracellular HMGB1 expression was significantly reduced in both the SDT and MBs + SDT groups because of the increased extracellular HMGB1 release induced by ICD. According to the flow cytometry analysis, the intracellular HMGB1 expression in HepG2 cells after SDT and MBs + SDT treatment decreased to approximately 35.43 ± 5.80 and 17.00 ± 1.77% ($p < 0.05$), respectively, compared to the untreated group (Figure 5D,F).

Consistent with the results of CRT expression and HMGB1 release, the highest level of extracellular ATP secretion was observed in cells from the MBs + SDT group relative to other treatments (Figure 5G). These results indicate that SDT treatment could induce immunogenic death of HepG2 cells in vitro and that MBs-triggered UTMD further enhanced ICD efficacy.

Evaluation of Antitumor Effect In Vivo. Encouraged by the enhanced antitumor results in vitro, the therapeutic efficacy of SDT combined with MBs was further evaluated in a Hepa1−6 tumor-bearing mice model (Figure 6A). As shown in Figure 6B, the tumors in the control group continued to grow rapidly within 14 days, and treatment with US or DVDMS alone did not demonstrate obvious antitumor effects (all, $p > 0.05$). MBs + US treatment demonstrated a mild tumor suppressive effect ($p > 0.05$). Both SDT and MBs + SDT treatment significantly suppressed tumor growth ($p < 0.05$). Notably, the MBs + SDT group demonstrated a smaller tumor volume, demonstrating that MBs contribute to SDT efficacy in vivo (Figure 6C). The weight of the mice exhibited no major changes in either the control or different treatment groups during the experiments, indicating negligible systemic toxicity of the treatments (Figure 6D). The tumors were then removed and stained with H&E, TUNEL, and Ki67 to confirm therapeutic efficacy (Figure 6E). According to the H&E staining results, the control, US, and DVDMS-treated groups exhibited normal morphology; the MBs + US group demonstrated mild tissue damage, whereas the SDT and MBs + SDT groups exhibited severe tissue damage. Similarly, the TUNEL assay revealed stronger apoptosis in the MBs + SDT group than in the SDT group, with almost no apoptosis observed in other groups (Figure S2A). Moreover, Ki67 staining results demonstrated that SDT and MBs + SDT treatment effectively inhibited tumor cell proliferation (Figure S2B). Taken together, our results demonstrated the ability of MBs to enhance the therapeutic effect of SDT in vivo.

DISCUSSION

Sonodynamic therapy is a cancer treatment with great clinical application value, high biocompatibility, and deep tissue permeability.[51,52] Low-intensity ultrasound is used in SDT to activate sonosensitizers and generate excessive ROS, leading to tumor cell inhibition and apoptosis.[53,54] Additionally, SDT has demonstrated synergistic anticancer effects with other therapies, such as photodynamic therapy and chemotherapy.[55,56] Currently, improving drug delivery and increasing drug enrichment within tumor cells are key challenges for tumor therapies. According to Sauerwein's book, neutron capture therapy uses the high propensity of the nonradioactive nuclides to capture thermal neutrons, resulting in prompt nuclear reaction.[57] Therefore, developing boron and gadolinium carrier compounds is essential for selectively delivering sufficient amounts of ^{10}B and ^{157}Gd into tumor cells for neutron capture therapy.[58] Similarly, increasing the uptake of sonosensitizers by tumor cells also contributes to improving the therapeutic efficacy of SDT. The development of nanomaterials has facilitated drug delivery and targeted release, increasing the concentration of therapeutic agents at the tumor site and avoiding damage to surrounding normal tissue.[59] In this study, we used MBs to increase the uptake of sonosensitizer by tumor cells. Ultrasound-targeted microbubble destruction (UTMD) has been used in multiple studies to inhibit tumor progression by destroying tumor blood vessels.[60,61] As a commonly used contrast-enhanced agent to improve ultrasound imaging, MBs are characterized by high safety and stability and have been validated to improve drug delivery by augmenting plasma membrane permeability.[62,63] Our experimental results demonstrated that MBs combined with US can effectively increase the accumulation of DVDMS in HepG2 cells (Figure S1).

https://doi.org/10.1021/acsomega.4c07746
ACS Omega 2024, 9, 51253−51263

It was reported that MBs combined with SDT efficiently killed cancer cells and induced apoptosis. Wang et al. demonstrated the combination of clinically approved MBs SonoVue and SDT treatment for enhancing cell cytotoxicity and improving tumor tissue destruction for colon cancer.[64] This study used an ultrasound contrast agent, Feriview, which was independently developed by Chinese scholars and is currently undergoing phase 3 clinical trials. Moreover, our research further investigated the mechanisms by which MBs combined with SDT increased ROS production. Previous studies indicated that DVDMS can be effectively absorbed by HepG2 cells, reaching maximum uptake after 5 h of incubation, whereas normal hepatocytes metabolize it within 4−9 h.[44] Therefore, the optimal incubation time of DVDMS with HepG2 cells before sono-irradiation was set at 5 h in our experiment. Results in Figure 2 demonstrated notable amounts of ROS generated after SDT + MBs treatment, both in vitro and in solution. On one hand, the cavitation effect produced by MBs under US irradiation enhanced cell permeability, which increased the cellular uptake of DVDMS; on the other hand, the UTMD process could also promote ROS production. Thus, our experimental results suggest that the introduction of MBs during SDT further increases intracellular ROS production.

In addition to the ROS-based cytotoxicity induced by SDT, MBs may also enhance the mechanical damage caused by US to tumor cells, contributing to cell necrosis. As shown in Figure 3, the cytotoxic effects of DVDMS-mediated SDT on HepG2 cells were concentration-dependent. The addition of MBs further increased cytotoxicity compared to SDT alone. Calcein AM/PI staining further confirmed the antitumor effectiveness of SDT and MBs. The reported study has shown that DVDMS localizes subcellularly to mitochondria, while increased ROS production is often associated with mitochondrial dysfunction.[65] Our previous work also demonstrated the involvement of mitochondrial membrane depolarization in SDT-induced cell apoptosis.[66] In the present study, the most significant apoptosis was observed in the MBs + SDT group (Figure 4), indicating that MBs may contribute to the mechanical damage caused by SDT in tumor cells and induce cell apoptosis. Similarly, the study by Xie et al. also demonstrated that MBs combined with SDT could increase the apoptosis rate of cancer cells. Notably, we have further investigated the role of other kinds of cell death, in addition to apoptosis, in treating liver cancer.[67]

Recent studies have reported that SDT not only directly kills cancer cells but also induces an ICD effect.[68,69] During SDT, sonosensitizers activated by US are utilized to generate ROS for direct killing or induction of tumor cell apoptosis, and the destruction of tumor cells leads to the production and secretion of tumor-associated antigens.[70,71] Uptake of antigens by dendritic cells (DC) in the presence of immunostimulatory cytokines leads to the development of anticancer effects by cytotoxic T lymphocytes (CTLs).[47,72] Moreover, UTMD was reported to induce endoplasmic reticulum stress, triggering ICD and releasing multiple danger-associated molecular patterns (DAMPs).[50] Therefore, representative ICD markers, including CRT expressed on the tumor cell surface, released HMGB1, and secreted ATP, were detected in our experiment. As shown in Figure 5, both CRT exposure and nuclear HMGB1 release were significantly enhanced after SDT treatment and reached a maximum in the MBs + SDT group, consistent with the ICD. Similar to our results, Wu et al. prepared nanomaterials loaded with sonosensitizer IR780 for SDT treatment and observed an increase in the expression of CRT and HMGB1.[73] Moreover, the highest level of extracellular ATP was observed with the combination of MBs and SDT. Our results demonstrated that MBs-mediated UTMD further enhanced ICD induction in the SDT, consistent with a previous study.[74]

In addition to analyzing the effects of various treatments in vitro, tumor suppression was assessed in Hepa1−6 tumor-bearing mice. The results shown in Figure 6 clearly demonstrate the superiority of SDT and MBs + SDT treatment in inhibiting tumor growth compared to the other treatment groups. Consistent with the safety advantage of SDT, there was no remarkable change in mice weight in the different treatment groups compared to the control, suggesting that the anticancer approach had slight side effects. The results of H&E, TUNEL, and Ki67 staining further demonstrated the potential of MBs to promote SDT-induced cancer cell necrosis and apoptosis and inhibit tumor cell proliferation.

Our study had some limitations. First, we used subcutaneous tumor models and should focus on the treatment of orthotopic tumors in further studies. Second, the effects of ICD on immune cells, such as DC maturation, CTLs recruitment, and serum pro-inflammatory cytokine secretion, have not been validated.

CONCLUSIONS

The present study demonstrated the synergistic effect of MBs and DVDMS-mediated SDT, both in vitro and in vivo. Our data indicated that UTMD potentiated SDT-induced excessive ROS production, inhibition of cell proliferation, and apoptosis of HepG2 cells. Notably, we found that some tumor cells underwent ICD after SDT and MBs + SDT treatment, indicating that MBs can be used as synergistic agents in SDT for HCC treatment. Owing to the superior biosafety and wide clinical use of MBs, and SDT being noninvasive and effective in cancer treatment, we can expect MBs combined with SDT to be a promising clinical transformation strategy.

ASSOCIATED CONTENT

Supporting Information

The Supporting Information is available free of charge at https://pubs.acs.org/doi/10.1021/acsomega.4c07746.

Flow cytometry results of cellular uptake; quantitative analysis of TUNEL and Ki67 staining (PDF)

AUTHOR INFORMATION

Corresponding Authors

Zhifei Dai − *Department of Biomedical Engineering, College of Future Technology, National Biomedical Imaging Center, Peking University, Beijing 100871, China*; Email: zhifei.dai@pku.edu.cn

Xiuli Yue − *School of Environment, Harbin Institute of Technology, Harbin, Heilongjiang Province 150001, China*; Email: xiulidx@163.com

Wen Cheng − *Department of Ultrasound, Harbin Medical University Cancer Hospital, Harbin, Heilongjiang Province 150081, China*; orcid.org/0000-0003-4294-9698; Email: hrbchengwen@163.com

https://doi.org/10.1021/acsomega.4c07746
ACS Omega 2024, 9, 51253−51263

Authors

Huajing Yang − *Department of Ultrasound, Harbin Medical University Cancer Hospital, Harbin, Heilongjiang Province 150081, China*

Yunfeng Qu − *Department of Biomedical Engineering, College of Future Technology, National Biomedical Imaging Center, Peking University, Beijing 100871, China*

Yuhang Tian − *Department of Ultrasound, Harbin Medical University Cancer Hospital, Harbin, Heilongjiang Province 150081, China*

Chunyue Wang − *Department of Ultrasound, Harbin Medical University Cancer Hospital, Harbin, Heilongjiang Province 150081, China*

Yucao Sun − *Department of Ultrasound, Harbin Medical University Cancer Hospital, Harbin, Heilongjiang Province 150081, China*

Complete contact information is available at: https://pubs.acs.org/10.1021/acsomega.4c07746

Author Contributions

H.Y.: Data curation and writing−original draft. Z.D.: Conceptualization and methodology. Y.Q.: Software. Y.T.: Investigation, Resources. C.W.: Formal analysis and project administration. Y.S.: Validation and visualization. W.C.: Funding acquisition and Writing−review and editing. X.Y.: Funding acquisition and supervision. All authors agreed on the journal to which the article would be submitted, gave final approval of the version to be published, and agreed to be accountable for all aspects of this study.

Funding

This research was supported by the National Natural Science Foundation of China (Grant 82171947 to W.C. and Grant 82071980 to X.L.Y.), the Heilongjiang Provincial Natural Science Foundation of China (grant number ZD2021H005), and the Interdisciplinary Research Foundation of HIT.

Notes

The authors declare no competing financial interest.

■ ACKNOWLEDGMENTS

We thank the flow cytometry Core at the National Center for Protein Sciences at Peking University for the technical help.

■ REFERENCES

(1) Sung, H.; Ferlay, J.; Siegel, R. L.; et al. Global Cancer Statistics 2020: GLOBOCAN Estimates of Incidence and Mortality Worldwide for 36 Cancers in 185 Countries. *CA Cancer J. Clin.* **2021**, *71* (3), 209−249.

(2) Vogel, A.; Meyer, T.; Sapisochin, G.; Salem, R.; Saborowski, A. Hepatocellular carcinoma. *Lancet.* **2022**, *400* (10360), 1345−1362.

(3) Cabibbo, G.; Enea, M.; Attanasio, M.; Bruix, J.; Craxì, A.; Cammà, C. A meta-analysis of survival rates of untreated patients in randomized clinical trials of hepatocellular carcinoma. *Hepatology.* **2010**, *51* (4), 1274−1283.

(4) Singal, A. G.; Kudo, M.; Bruix, J. Breakthroughs in Hepatocellular Carcinoma Therapies. *Clin Gastroenterol Hepatol.* **2023**, *21* (8), 2135−2149.

(5) Yang, C.; Zhang, H.; Zhang, L.; et al. Evolving therapeutic landscape of advanced hepatocellular carcinoma. *Nat. Rev. Gastroenterol Hepatol.* **2023**, *20* (4), 203−222.

(6) Finn, R. S.; Zhu, A. X. Evolution of Systemic Therapy for Hepatocellular Carcinoma. *Hepatology* **2021**, *73* (Suppl 1), 150−157.

(7) Yumita, N.; Sasaki, K.; Umemura, S.; Yukawa, A.; Nishigaki, R. Sonodynamically induced antitumor effect of gallium-porphyrin complex by focused ultrasound on experimental kidney tumor. *Cancer Lett.* **1997**, *112* (1), 79−86.

(8) Canaparo, R.; Foglietta, F.; Barbero, N.; Serpe, L. The promising interplay between sonodynamic therapy and nanomedicine. *Adv. Drug Deliv Rev.* **2022**, *189*, No. 114495.

(9) Cao, X.; Li, M.; Liu, Q.; Zhao, J.; Lu, X.; Wang, J. Inorganic Sonosensitizers for Sonodynamic Therapy in Cancer Treatment. *Small* **2023**, *19*, No. 2303195.

(10) Li, X.; Geng, X.; Chen, Z.; Yuan, Z. Recent advances in glioma microenvironment-response nanoplatforms for phototherapy and sonotherapy. *Pharmacol. Res.* **2022**, *179*, No. 106218.

(11) Wang, X.; Xu, X.; Yang, Z.; et al. Improvement of the effectiveness of sonodynamic therapy: by optimizing components and combination with other treatments. *Biomater Sci.* **2023**, *11* (23), 7489−7511.

(12) Lv, L.; Zhang, J.; Wang, Y.; et al. Boron neutron capture therapy-derived extracellular vesicles via DNA accumulation boost antitumor dendritic cell vaccine efficacy. *Adv. Sci. (Weinh)* **2024**, *11* (35), No. 2405158.

(13) Wang, Z.; Lei, R.; Zhang, Z.; et al. Boron-containing MOF nanoparticles with stable metabolism in U87-MG cells combining microdosimetry to evaluate relative biological effectiveness of boron neutron capture therapy. *ACS Appl. Mater. Interfaces.* **2024**, *16* (3), 3232−3242.

(14) Hosmane, N. S. *Boron and gadolinium neutron capture therapy for cancer treatment*; World Scientific, 2012.

(15) Pan, X.; Wang, H.; Wang, S.; et al. Sonodynamic therapy (SDT): a novel strategy for cancer nanotheranostics. *Sci. China Life Sci.* **2018**, *61* (4), 415−426.

(16) Pan, M.; Hu, D.; Yuan, L.; et al. Newly developed gas-assisted sonodynamic therapy in cancer treatment. *Acta Pharm. Sin B* **2023**, *13* (7), 2926−2954.

(17) Lin, J.; Li, D.; Li, C.; et al. A review on reactive oxygen species (ROS)-inducing nanoparticles activated by uni- or multi-modal dynamic treatment for oncotherapy. *Nanoscale.* **2023**, *15* (28), 11813−11833.

(18) Zhang, Y.; Yu, W.; Chen, M.; Zhang, B.; Zhang, L.; Li, P. The applications of nanozymes in cancer therapy: based on regulating pyroptosis, ferroptosis and autophagy of tumor cells. *Nanoscale.* **2023**, *15* (29), 12137−12156.

(19) Zhang, C.; Pu, K. Organic Sonodynamic Materials for Combination Cancer Immunotherapy. *Adv. Mater.* **2023**, *35*, No. 2303059.

(20) Liao, S.; Cai, M.; Zhu, R.; et al. Antitumor Effect of Photodynamic Therapy/Sonodynamic Therapy/Sono-Photodynamic Therapy of Chlorin e6 and Other Applications. *Mol. Pharmaceutics* **2023**, *20* (2), 875−885.

(21) Fang, Q.; Yang, D. A porphyrin dimmer combined with the ether bond and its manufacturing method. Patent in China; ZL200910179116.5, 2012.

(22) Hu, J.; Wang, X.; Zhang, K.; et al. Sinoporphyrin sodium: a novel sensitizer in sonodynamic therapy. *Anticancer Drugs.* **2014**, *25* (2), 174−182.

(23) Liu, Y.; Bai, L.; Guo, K.; et al. Focused ultrasound-augmented targeting delivery of nanosonosensitizers from homogenous exosomes for enhanced sonodynamic cancer therapy. *Theranostics.* **2019**, *9* (18), 5261−5281.

(24) Yao, J.; Yang, Z.; Huang, L.; et al. Low-Intensity Focused Ultrasound-Responsive Ferrite-Encapsulated Nanoparticles for Atherosclerotic Plaque Neovascularization Theranostics. *Adv. Sci. (Weinh)* **2021**, *8* (19), No. 2100850.

(25) Jia, M. G.; Wu, H. Y.; Sun, L. L.; et al. Analysis of porphyrin photosensitizers using HPLC method. *Yao Xue Xue Bao* **2015**, *50* (8), 1021−1025.

(26) Nowak, K. M.; Schwartz, M. R.; Breza, V. R.; Price, R. J. Sonodynamic therapy: Rapid progress and new opportunities for non-invasive tumor cell killing with sound. *Cancer Lett.* **2022**, *532*, No. 215592.

(27) Jeong, S. D.; Jung, B. K.; Ahn, H. M.; et al. Immunogenic Cell Death Inducing Fluorinated Mitochondria-Disrupting Helical Polypeptide Synergizes with PD-L1 Immune Checkpoint Blockade. *Adv. Sci. (Weinh)* **2021**, *8* (7), No. 2001308.
(28) He, M.; Wang, M.; Xu, T.; et al. Reactive oxygen species-powered cancer immunotherapy: Current status and challenges. *J. Controlled Release* **2023**, *356*, 623−648.
(29) Tan, X.; Huang, J.; Wang, Y.; et al. Transformable Nanosensitizer with Tumor Microenvironment-Activated Sonodynamic Process and Calcium Release for Enhanced Cancer Immunotherapy. *Angew. Chem., Int. Ed. Engl.* **2021**, *60* (25), 14051−14059.
(30) Zeng, Z.; Zhang, C.; He, S.; Li, J.; Pu, K. Activatable Cancer Sono-Immunotherapy using Semiconducting Polymer Nanobodies. *Adv. Mater.* **2022**, *34* (28), No. 2203246.
(31) Shen, K. Y.; Zhu, Y.; Xie, S. Z.; et al. Immunosuppressive tumor microenvironment and immunotherapy of hepatocellular carcinoma: current status and prospectives. *J. Hematol. Oncol.* **2024**, *17* (1), 25.
(32) Han, Y.; Sun, J.; Wei, H.; Hao, J.; Liu, W.; Wang, X. Ultrasound-Targeted Microbubble Destruction: Modulation in the Tumor Microenvironment and Application in Tumor Immunotherapy. *Front Immunol.* **2022**, *13*, No. 937344.
(33) Ai, C.; Sun, X.; Xiao, S.; et al. CAFs targeted ultrasound-responsive nanodroplets loaded V9302 and GLULsiRNA to inhibit melanoma growth via glutamine metabolic reprogramming and tumor microenvironment remodeling. *J. Nanobiotechnol.* **2023**, *21* (1), 214.
(34) Arulpragasam, A. R.; van't Wout-Frank, M.; Barredo, J.; Faucher, C. R.; Greenberg, B. D.; Philip, N. S. Low Intensity Focused Ultrasound for Non-invasive and Reversible Deep Brain Neuromodulation-A Paradigm Shift in Psychiatric Research. Front. *Psychiatry.* **2022**, *13*, No. 825802.
(35) Fan, P.; Yang, D.; Wu, J.; et al. Cell-cycle-dependences of membrane permeability and viability observed for HeLa cells undergoing multi-bubble-cell interactions. *Ultrason Sonochem.* **2019**, *53*, 178−186.
(36) Szablowski, J. O.; Bar-Zion, A.; Shapiro, M. G. Achieving Spatial and Molecular Specificity with Ultrasound-Targeted Biomolecular Nanotherapeutics. *Acc. Chem. Res.* **2019**, *52* (9), 2427−2434.
(37) Liang, J.; Qiao, X.; Qiu, L.; et al. Engineering Versatile Nanomedicines for Ultrasonic Tumor Immunotherapy. *Adv. Sci. (Weinh)* **2024**, *11* (3), No. 2305392.
(38) Sun, S.; Wang, P.; Sun, S.; et al. Applications of Micro/Nanotechnology in Ultrasound-based Drug Delivery and Therapy for Tumor. *Curr. Med. Chem.* **2021**, *28* (3), 525−547.
(39) Beekers, I.; Langeveld, S.; Meijlink, B.; et al. Internalization of targeted microbubbles by endothelial cells and drug delivery by pores and tunnels. *J. Controlled Release* **2022**, *347*, 460−475.
(40) Jang, Y.; Park, J.; Kim, P.; et al. Development of exosome membrane materials-fused microbubbles for enhanced stability and efficient drug delivery of ultrasound contrast agent. *Acta Pharm. Sin B* **2023**, *13* (12), 4983−4998.
(41) Song, L.; Wang, G.; Hou, X.; et al. Biogenic nanobubbles for effective oxygen delivery and enhanced photodynamic therapy of cancer. *Acta Biomater.* **2020**, *108*, 313−325.
(42) Chowdhury, S. M.; Abou-Elkacem, L.; Lee, T.; Dahl, J.; Lutz, A. M. Ultrasound and microbubble mediated therapeutic delivery: Underlying mechanisms and future outlook. *J. Controlled Release* **2020**, *326*, 75−90.
(43) Stribbling, S. M.; Ryan, A. J. The cell-line-derived subcutaneous tumor model in preclinical cancer research. *Nat. Protoc.* **2022**, *17* (9), 2108−2128.
(44) Li, E.; Sun, Y.; Lv, G.; et al. Sinoporphyrin sodium based sonodynamic therapy induces anti-tumor effects in hepatocellular carcinoma and activates p53/caspase 3 axis. *Int. J. Biochem. Cell Biol.* **2019**, *113*, 104−114.
(45) Cai, L.; Qin, X.; Xu, Z.; et al. Comparison of cytotoxicity evaluation of anticancer drugs between real-time cell analysis and CCK-8 method. *ACS Omega.* **2019**, *4* (7), 12036−12042.
(46) Zhang, G.; Gurtu, V.; Kain, S. R.; et al. Early detection of apoptosis using a fluorescent conjugate of annexin V. *Biotechniques.* **1997**, *23* (3), 525−531.
(47) Chen, L.; Xue, W.; Cao, J.; et al. TiSe2-mediated sonodynamic and checkpoint blockade combined immunotherapy in hypoxic pancreatic cancer. *J. Nanobiotechnol.* **2022**, *20* (1), 453.
(48) Li, T.; Lv, H.; Yang, L.; et al. Pharmacokinetics and tissue distribution of DVDMS-2 in tumor-bearing mice. *Photochem. Photobiol.* **2020**, *96* (1), 148−155.
(49) Kamel, A. G.; Sabet, S.; El-Shibiny, A. Potential mitochondrial ROS-mediated damage induced by chitosan nanoparticles bee venom-loaded on cancer cell lines. *Int. J. Biol. Macromol.* **2024**, *279* (Pt 4), No. 135362.
(50) Wang, X.; Li, F.; Zhang, J.; et al. A combination of PD-L1-targeted IL-15 mRNA nanotherapy and ultrasound-targeted microbubble destruction for tumor immunotherapy. *J. Controlled Release* **2024**, *367*, 45−60.
(51) He, Z.; Du, J.; Miao, Y.; Li, Y. Recent Developments of Inorganic Nanosensitizers for Sonodynamic Therapy. *Adv. Healthc. Mater.* **2023**, *12*, No. 2300234.
(52) Jiang, J.; Zhang, M.; Lyu, T.; et al. Sono-Driven STING Activation using Semiconducting Polymeric Nanoagonists for Precision Sono-Immunotherapy of Head and Neck Squamous Cell Carcinoma. *Adv. Mater.* **2023**, *35* (30), No. 2300854.
(53) Hu, H.; Zhao, J.; Ma, K.; et al. Sonodynamic therapy combined with phototherapy: Novel synergistic strategy with superior efficacy for antitumor and antiinfection therapy. *J. Controlled Release* **2023**, *359*, 188−205.
(54) Zheng, Y.; Ye, J.; Li, Z.; Chen, H.; Gao, Y. Recent progress in sono-photodynamic cancer therapy: From developed new sensitizers to nanotechnology-based efficacy-enhancing strategies. *Acta Pharm. Sin B* **2021**, *11* (8), 2197−2219.
(55) Liu, Z.; Li, J.; Chen, W.; Liu, L.; Yu, F. Light and sound to trigger the Pandora's box against breast cancer: A combination strategy of sonodynamic, photodynamic and photothermal therapies. *Biomaterials.* **2020**, *232*, No. 119685.
(56) Fan, Y.; Xu, P.; Fang, Q.; et al. Biomimetic Nanoparticle with Glutathione Depletion and Amplified ROS Generation Capabilities for Synergistic Chemo-Sonodynamic Therapy in Squamous Cell Carcinomas. *ACS Appl. Mater. Interfaces.* **2023**, *15* (22), 27183−27194.
(57) Sauerwein, W. A. G., Eds. *Neutron capture therapy: principles and applications*; Springer Science and Business Media, 2012.
(58) Mi, P.; Dewi, N.; Yanagie, H.; et al. Hybrid Calcium Phosphate-Polymeric Micelles Incorporating Gadolinium Chelates for Imaging-Guided Gadolinium Neutron Capture Tumor Therapy. *ACS Nano* **2015**, *9* (6), 5913−5921.
(59) Huang, Y.; Ouyang, W.; Lai, Z.; et al. Nanotechnology-enabled sonodynamic therapy against malignant tumors. *Nanoscale Adv.* **2024**, *6* (8), 1974−1991.
(60) Zhao, Y.; Shi, D.; Guo, L.; et al. Ultrasound targeted microbubble destruction-triggered nitric oxide release via nanoscale ultrasound contrast agent for sensitizing chemoimmunotherapy. *J. Nanobiotechnol.* **2023**, *21* (1), 35.
(61) He, Y.; Dong, X. H.; Zhu, Q.; Xu, Y. L.; Chen, M. L.; Liu, Z. Ultrasound-triggered microbubble destruction enhances the radiosensitivity of glioblastoma by inhibiting PGRMC1-mediated autophagy in vitro and in vivo. *Mil. Med. Res.* **2022**, *9* (1), 9.
(62) Wu, N.; Cao, Y.; Liu, Y.; et al. Low-intensity focused ultrasound targeted microbubble destruction reduces tumor blood supply and sensitizes anti-PD-L1 immunotherapy. *Front. Bioeng. Biotechnol.* **2023**, *11*, No. 1173381.
(63) Fan, C. H.; Wu, N.; Yeh, C. K. Enhanced sonodynamic therapy by carbon dots-shelled microbubbles with focused ultrasound. *Ultrason Sonochem.* **2023**, *94*, No. 106342.
(64) Wang, H.; Wang, P.; Li, L.; et al. Microbubbles enhance the antitumor effects of sinoporphyrin sodium Mmediated sonodynamic therapy both in vitro and in vivo. *Int. J. Biol. Sci.* **2015**, *11* (12), 1401−1409.

https://doi.org/10.1021/acsomega.4c07746
ACS Omega 2024, 9, 51253−51263

(65) Shen, Y.; Chen, Y.; Huang, Y.; et al. An in vitro study on the antitumor effect of sonodynamic therapy using sinoporphyrin sodium on human glioblastoma cells. *Ultrasonics* **2021**, *110*, No. 106272.
(66) Yang, H.; Jing, H.; Han, X.; et al. Synergistic Anticancer Strategy of Sonodynamic Therapy Combined with PI-103 Against Hepatocellular Carcinoma. *Drug Des Devel Ther* **2021**, *15*, 531−542.
(67) Xie, R.; Xu, T.; Zhu, J.; et al. The Combination of Glycolytic Inhibitor 2-Deoxyglucose and Microbubbles Increases the Effect of 5-Aminolevulinic Acid-Sonodynamic Therapy in Liver Cancer Cells. *Ultrasound Med. Biol.* **2017**, *43* (11), 2640−2650.
(68) Wang, Y.; Gong, F.; Han, Z.; et al. Oxygen-Deficient Molybdenum Oxide Nanosensitizers for Ultrasound-Enhanced Cancer Metalloimmunotherapy. *Angew. Chem., Int. Ed. Engl.* **2023**, *62* (9), No. e202215467.
(69) Yang, Y.; Huang, J.; Liu, M.; et al. Emerging Sonodynamic Therapy-Based Nanomedicines for Cancer Immunotherapy. *Adv. Sci. (Weinh)* **2023**, *10* (2), No. 2204365.
(70) Ding, M.; Zhang, Y.; Yu, N.; et al. Augmenting Immunogenic Cell Death and Alleviating Myeloid-Derived Suppressor Cells by Sono-Activatable Semiconducting Polymer Nanopartners for Immunotherapy. *Adv. Mater.* **2023**, *35*, No. 2302508.
(71) Liang, S.; Yao, J.; Liu, D.; Rao, L.; Chen, X.; Wang, Z. Harnessing Nanomaterials for Cancer Sonodynamic Immunotherapy. *Adv. Mater.* **2023**, *35*, No. 2211130.
(72) Zhivaki, D.; Kagan, J. C. Innate immune detection of lipid oxidation as a threat assessment strategy. *Nat. Rev. Immunol.* **2022**, *22* (5), 322−330.
(73) Wu, W.; Xu, M.; Qiao, B.; et al. Nanodroplet-enhanced sonodynamic therapy potentiates immune checkpoint blockade for systemic suppression of triple-negative breast cancer. *Acta Biomater* **2023**, *158*, 547−559.
(74) Nesbitt, H.; Logan, K.; Thomas, K.; et al. Sonodynamic therapy complements PD-L1 immune checkpoint inhibition in a murine model of pancreatic cancer. *Cancer Lett.* **2021**, *517*, 88−95.

https://doi.org/10.1021/acsomega.4c07746
ACS Omega 2024, 9, 51253−51263